This is an open access article published under an ACS AuthorChoice License, which permits copying and redistribution of the article or any adaptations for non-commercial purposes.

ACS AUTHORCHOICE

ACS OMEGA

http://pubs.acs.org/journal/acsodf

Article

Role of Surface Acidity in the Surface Stabilization of the High-Voltage Cathode $LiNi_{0.6}Mn_{0.2}Co_{0.2}O_2$

Nathan D. Phillip,* Beth L. Armstrong, Claus Daniel, and Gabriel M. Veith*

Cite This: *ACS Omega* 2020, 5, 14968−14975

Read Online

ACCESS | Metrics & More | Article Recommendations | Supporting Information

ABSTRACT: Metal oxide coatings have been reported to be an effective approach for stabilizing cathode interfaces, but the associated chemistry is unclear. In this work, thin films of TiO_2, ZnO, and Cr_2O_3, which have different surface acidities/basicities, were used to modify the surface chemistry of $LiNi_{0.6}Mn_{0.2}Co_{0.2}O_2$ and study the acidity's role in the cathode/electrolyte interphase composition and impedance under high-voltage cycling (4.5 V *vs* Li/Li^+). Cathodes with more acidic surfaces provided higher initial specific capacity and capacity retention with cycling. More basic surfaces had higher initial impedance and greater impedance growth with cycling. These differences appeared to depend on the degree of $LiPF_6$ salt decomposition at the interface, which was related to acidity, with more neutral surfaces having a $LiF/Li_xPO_yF_z$ ratio close to unity, but basic surfaces had substantially more LiF. This chemistry was more significant than the cathode electrolyte interphase (CEI) thickness as the more acidic surfaces formed a thicker CEI than the basic surface, resulting in better capacity retention. These results suggest that the Brønsted acidity of cathodes directly influences electrolyte degradation, ion transport, and thus, cell lifetime.

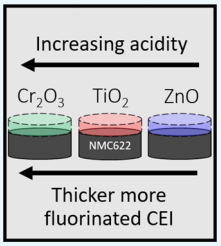

■ INTRODUCTION

Inorganic coatings of metal oxides are a common mitigation strategy for stabilizing lithium-ion battery cathode interfaces which degrade during operation at high voltages (≥4.5 V *vs* Li/Li^+). Thin layers (up to tens of nm) of Al_2O_3,[1−3] TiO_2,[4−6] Cr_2O_3,[7,8] and ZnO[9,10] have been coated on the surface of the cathode active materials before electrode preparation. Deposition methods include atomic layer deposition,[3] sol−gel synthesis,[2] hydrolyzation,[4] and physical vapor deposition,[11] and the coatings are reported to reduce charge-transfer impedance rise during cycling and extend cell cycle life by suppressing electrolyte decomposition.[10,12−14] The cause of this stabilization is often attributed to scavenging HF, suppressing transition metal dissolution, and preventing contact between the electrolyte and the active material surface.[4,10,13,14] The mechanisms involved remain a subject of ongoing study, although synergies between surface coatings and electrolyte decomposition have been observed, such as Al_2O_3 reacting with $LiPF_6$ salt to form a passivating layer of AlF_3 at the interface and the beneficial additive $LiPO_2F_2$ in the electrolyte.[15]

The relationship between these metal oxide coatings to electrolyte decomposition is not well understood for cathode materials such as Ni-rich NMC ($LiNi_xMn_yCo_zO_2$, where $x + y + z = 1$ and $x > 0.5$) cycled to high upper cutoff voltages (*e.g.*, 4.5 V *vs* Li^+/Li) for additional capacity. Electrolyte decomposition coupled with structural rearrangement (*i.e.* layered $R\bar{3}m$ to rock salt)[16] prevents commercial operation of these materials at high voltages, so understanding how coatings might stabilize the cathode electrolyte interphase (CEI) would inform cell designs for increased energy density of these promising materials. A rough 25−35 nm layer of anatase TiO_2 was shown to improve the rate capability of NMC622 cycled to 4.5 V *versus* Li/Li^+ and was attributed to reduced impedance growth because of suppression of interfacial reactions and reduced cation mixing in the bulk structure of the pristine material.[4] Surface doping of Ti^{4+} in NMC622 with a nanosized coating of TiO_2 was also found to reduce film impedance over additional cycles to 4.4 V *versus* Li/Li^+.[5,6] Cr_2O_3 has been deposited on NMC111 to improve the rate capability at 3 C and structural integrity at high temperatures[7] and suppress Mn^{2+} dissolution from spinel $LiMn_2O_4$.[8] Similarly, metal dissolution from $LiNi_{0.8}Co_{0.15}Al_{0.05}O_2$ was reduced when coated with 20 nm sputtered films of ZnO which minimized impedance rise because of the coating.[10] While these surface coatings are often amorphous, it is worth noting that crystallinity, cation valence, and the chemical stability of oxide coatings all contribute to the interfacial environment.

Studying interfacial phenomena related to the cathode active material in composite electrodes is challenging because of potential interactions between the metal oxide coatings and the binder, conductive carbon, and conductive graphite. To reduce the complexity of the system of interest (the electrolyte/metal oxide/cathode interface), thin film electrodes solely comprising the cathode active material can be used as a model environment. The fully dense film removes the need for

Received: February 1, 2020
Accepted: June 3, 2020
Published: June 17, 2020

Downloaded via 207.241.233.158 on November 1, 2020 at 07:51:03 (UTC).
See https://pubs.acs.org/sharingguidelines for options on how to legitimately share published articles.

© 2020 American Chemical Society

https://dx.doi.org/10.1021/acsomega.0c00458
ACS Omega 2020, 5, 14968−14975

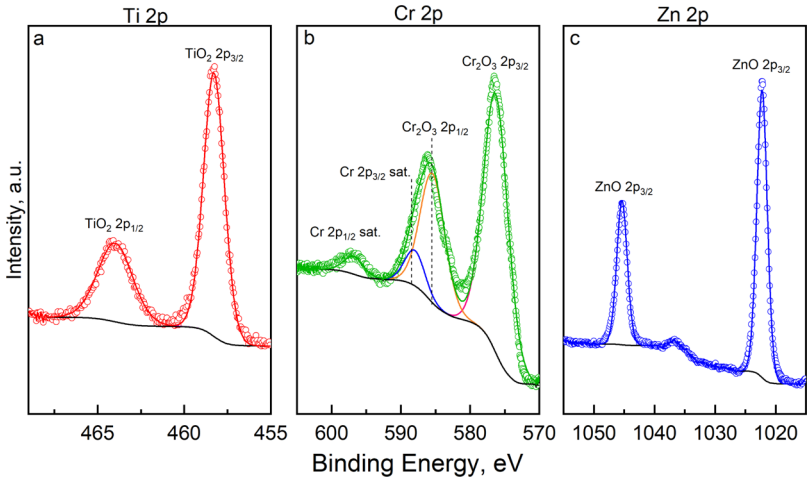

Figure 1. XPS spectra of pristine M−O coatings of (a) Ti 2p, (b) Cr 2p, and (c) Zn 2p on NMC622.

binders, conductive carbon, and slurry processing variations, as well as enables the planar geometry for simplified electrochemical impedance analysis and direct control of the interfacial environment.[17] Depositing a thin layer of metal oxide atop a thin film cathode provides a well-defined environment for studying interactions between the cathode, metal oxide, and the electrolyte.

The surfaces of all metal oxides are terminated by hydroxyl groups, and the adsorption of species in air may lead to additional surface groups such as CO_3^{2-} from adsorbed CO_2.[18] This surface termination is the origin of acid/base properties of metal oxides and governs the charge transfer reaction of the electric double layer, as well as influences slurry processing efficacy to make electrodes,[19] so it is useful to study model environments to avoid complex slurry and binder interactions influencing the modified interface. The intrinsic surface charge varies between metal oxides and can be described by their point of zero surface charge or isoelectric point (IEP).[19,20] Increased hydroxylation of NMC cathode surfaces is predicted to increase the reaction energy barrier for ethylene carbonate (EC) decomposition based on modeling studies.[21] The ring opening decomposition reaction of EC was theoretically found to be impeded by NMC surfaces with more M−OH groups compared to the M−F and O−H surface models.[21] It was hypothesized that different acidities of the surface −OH groups might explain the influence of metal oxide coatings on the CEI. This also might offer insight into how the initial surface chemistry on the interface of pristine NMC622 influences cycling stability.[22] Paulsen *et al.* observed that the initial surface chemistry of NMC can be characterized by the "soluble base content" (SBC) or the amount of LiOH and Li_2CO_3 formed on the surface during reaction with water.[22] They found an optimum range for Ni-rich NMC materials at 80−120 μmol/g SBC, indicating that having a complex initial surface chemistry is more beneficial to cycling than neat NMC.[22] By selecting coatings with different IEP values, the initial surface chemistry can be modified (*i.e.* acidity of terminating −OH). In this study, the relationship of surface charge to the formation of species in the CEI was investigated by controlling the NMC622 interface with thin metal oxide films. We chose metal oxides based on well-defined IEP's. This did not include Al_2O_3 because of its amphoteric nature.

■ RESULTS AND DISCUSSION

Three metal oxides were selected to modify the surface charge of NMC622. Cr_2O_3 was chosen to induce a more acidic surface based on the low IEP (approximately pH of 2) reported for the powder and Cr_2O_3-coated particles.[8] ZnO served as a basic surface modification because of its higher IEP of 9.0−10.3, depending on the synthesis conditions.[20] TiO_2 was selected as a coating which would not modify the surface charge significantly because of its similar IEP to NMC622 (4.7−6.2).[20] Al_2O_3 was not selected for this study because of the wide range of IEP values reported (5.0−9.25), depending on phases and synthesis conditions.[20] It is to be noted that ZnO has different IEPs depending on the phase, but they are all in the basic range and far closer in value than the various Al_2O_3 phases. As reported previously, the films adopt a (104) orientation which we think plays a role in the observed electrochemical properties discussed below.[23]

These surface environments were established by depositing a thin layer of metal oxides onto NMC622 thin film cathodes by dc magnetron sputtering of Ti, Cr, or Zn in a reactive atmosphere (3:1 Ar/O_2). A quartz crystal microbalance measured the deposition rate such that 3 nm of TiO_2, Cr_2O_3, and ZnO could be deposited on the surface of NMC622 samples. Magnetron sputtering is a relatively low energy process where there should be minimal degradation of the surface from ion bombardment.[24] Furthermore, these depositions occurred at a much lower temperature than that for standard solution or ALD processing which involves heating to decompose a precursor or dry the sample, meaning any changes to the cathode/coating interface will be minimal. These coatings were examined with X-ray photoelectron spectroscopy (XPS), as shown in Figure 1, to determine the oxidation state of the metals to infer the metal oxide composition on the surface. Ti 2p spectra are shown in Figure 1a, where two sharp peaks were observed at 458.2 and 464.0 eV, corresponding to the orbital splitting of Ti $2p^{3/2}$ and Ti $2p^{1/2}$. The peak positions and separation of 5.8 eV corresponds to an oxidation state of Ti^{4+}, confirming a surface coating of TiO_2.[25] The Cr 2p spectra shows a similar orbital splitting in Figure 1b, with characteristic satellite lines appearing as shoulders to the primary peaks at 576.5 and 586.1 eV which match the peak positions of Cr^{3+} in Cr_2O_3.[25,26] The Zn 2p spectra appear at a higher binding energy, as seen in Figure 1c. Two sharp peaks at 1022.3 and 1045.4 eV indicate Zn^{2+} for the

https://dx.doi.org/10.1021/acsomega.0c00458
ACS Omega 2020, 5, 14968−14975

ZnO coating.[25] Ni 2p signals were still visible from the underlying cathode for each of these samples and are included in Figure S1. This indicates that the metal oxide coatings were sufficiently thin (∼3 nm) to not block photoelectrons emitted from the bulk cathode material. The surface of the cathodes mirrors the texture of the substrate which is composed of large flat facets of corundum.

To characterize how the chemical environment at the interface varied between metal oxide coatings, the zeta potential was calculated using a surface probe attachment. These data are included in Table 1 along with the measured IEP values for crystalline samples of the respective oxides powders. Crystalline powders of each of the metal oxides studied here were titrated over a pH range of ∼2−10. The IEP values in Table 1 were determined by measuring the zeta potential of the solution at each pH and interpolating the pH value where there was zero surface charge, as shown for each compound in Figure S2. The IEP of a compound can vary substantially between different crystal structures and preparation methods,[20,27] so the surface charges of sintered pellets of the same crystalline powders used for IEP measurements were compared to ∼200 nm of films sputtered on polycrystalline Al_2O_3 wafers at the same pH to determine whether they had comparable values. These were found to be in good agreement (±3.9 mV) with the exception of ZnO where the surface charge of the pellet was twice the magnitude of the film (see Table 1). This could be due to the crystalline nature of the pellet compared to the amorphous sputtered thin film or the concentration of surface −OH.

Table 1. Surface Charge for Sputtered Films on NMC622, Al_2O_3, Pellets of Pristine Metal Oxide Powders, and Measured IEP of Metal Oxide Powders Used in This Study

oxide	sample	surface zeta, mV	powder IEP
Cr_2O_3	3 nm on 1 μm NMC	−21.4	2.6
	200 nm on Al_2O_3	−11.0	
	pellet	−7.1	
TiO_2	3 nm on 1 μm NMC	−13.7	3.4
	230 nm on Al_2O_3	−28.7	
	pellet	−28.7	
NMC	1 μm	−9.2	3.5
ZnO	3 nm on 1 μm NMC	9.8	6.5
	200 nm on Al_2O_3	10.3	
	pellet	23.1	

Thin-film zeta potential measurements are dependent upon the competing effects of electrophoresis and electroosmosis of the solution at the surface and the tracer particles in the bulk solution. The zeta potential of the thin film surface (ζ_S) was calculated as the difference between the charge measured in the bulk solution (ζ_B, because of electrophoresis only) compared to that of the film/solution interface (ζ_W, because of electro-osmosis and electrophoresis). These values are determined by zeta potential measurements at increasing displacements from the surface (see Figure S3), where[28]

$$\zeta_S = \zeta_B - \zeta_W$$

For an accurate measurement, it is important to select a probing solution which matches the sign of the surface charge at the solution pH. For metal oxides with an IEP less than the pH of the probe solution, the negatively charged probe particle solution (Brookhaven Zeta Potential Reference, ZR5, pH 6.67) was selected, and for oxides with an IEP greater than the pH of the probe solution, the positively charged probe particle solution (Brookhaven Zeta Potential Reference, ZR6, pH 4.13) was selected. When a surface is immersed in a solution at a pH lower than the material's IEP, the surface will usually be positively charged, so a probing solution with positively

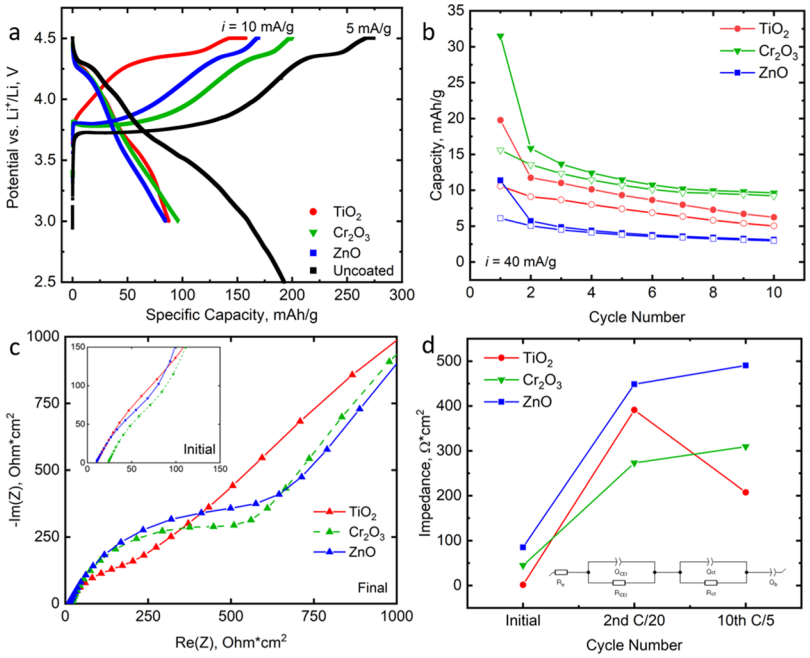

Figure 2. Electrochemical cycling of metal oxide-coated NMC622 *vs* Li metal at constant current/constant voltage (CC/CV) and baseline uncoated NMC622 from ref 33 for (a) the first cycle at 10 mA/g (∼C/20), (b) the specific capacity during 40 mA/g (∼C/5) cycles with solid and hollow symbols for charge and discharge capacity, respectively, (c) impedance measurements before cycling (inset) and after formation cycles and 40 mA/g cycles, and (d) growth of CEI impedance with cycling.

https://dx.doi.org/10.1021/acsomega.0c00458
ACS Omega 2020, 5, 14968−14975

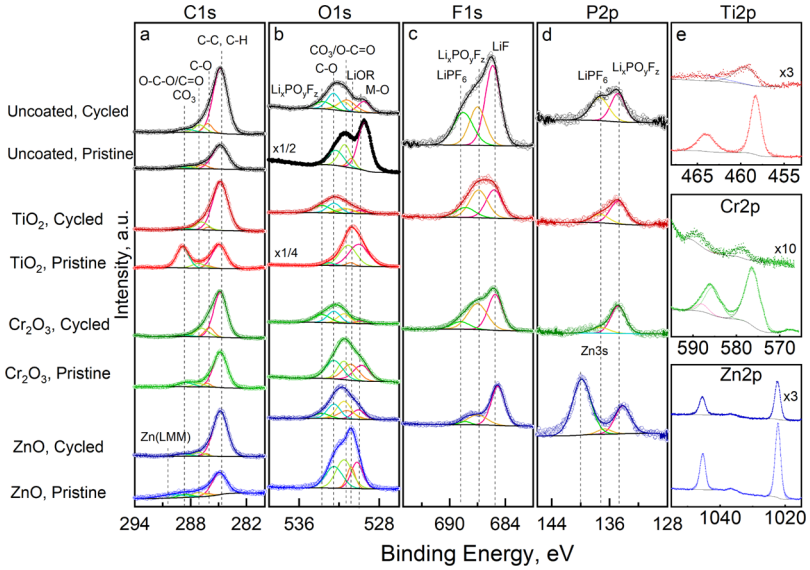

Figure 3. XPS spectra of pristine and metal oxide-coated NMC622 electrodes before and after two cycles and discharged to 3.0 V of (a) C 1s, (b) O 1s, (c) F 1s, (d) P 2p, and (e) Ti 2p, Cr 2p, and Zn 2p with certain spectra multiplied as indicated for clarity and uncoated NMC622 data included in black from ref 33.

charged probe particles must be selected so that the magnitude of electrostatic repulsion in the slipping plane (zeta potential) can be measured. This way, a surface is acidic or basic as well as the magnitude of the surface charge at that pH can be estimated.

The TiO_2-coated samples served as the baseline model in this study as a metal oxide coating with a similar surface zeta potential to that of uncoated NMC, which was expected because of the nearly identical IEP values of 3.4 and 3.5 for the powders measured here, as seen in Table 1. The Cr_2O_3-coated NMC films had a surface charge of 7.7 mV less than the TiO_2-coated samples, whereas the ZnO-coated samples were 23.5 mV greater. This variation is significant, given that the standard deviation was ±1.9 mV or less for each sample. The negatively charged surfaces originate dissociation of surface sites or adsorption of protons, whereas more positive values originate from basic groups such as hydroxyl groups that are known to terminate metal oxide surfaces.[19] The magnitude of zeta potential is based on the sum of the reactions of those surface groups at a given pH. As such, the Cr_2O_3-coated samples had more acidic sites or fewer basic groups than the TiO_2-coated films and the ZnO-coated films had more basic groups. These varied surface environments might impact the behavior of Li^+ solvation complexes at the interface and thus cell degradation, which will be discussed presently.

NMC622 half-cells were first cycled two times between 4.5 and 3.0 V *versus* Li/Li^+ at 10 mA/g (∼C/20); the first cycle specific capacity as a function of voltage is shown in Figure 2a. The overall structure of the voltage profile was similar between samples, with a plateau at 3.8 V corresponding to Ni^{2+}/Ni^{4+} redox. A secondary plateau at a higher voltage (∼4.4 V) has been attributed to the phase change and subsequent release of partial redox active oxygen species induced by cycling Ni-rich NMCs to high voltages.[29,30] Recently, thin films with preferred (104) crystal orientations were shown to have an exacerbated 4.4 V oxygen redox plateau in a liquid electrolyte but not in a solid-state configuration.[31] The TiO_2-coated samples have a suppressed 3.8 V plateau and an extended plateau at 4.4 V compared to the other two samples, indicating that this oxygen evolution reaction is promoted by the TiO_2 surface. The simultaneous suppression of the Ni redox plateau in the TiO_2-coated sample suggests that the underlying NMC cathode film has been modified or that the surface is more active toward the decomposition of the layered structure because of a rock-salt-like structure formation. Compared to the baseline NMC, the ZnO- and Cr_2O_3-coated samples have suppressed the 4.4 V plateau, whereas TiO_2 promoted it. The modification of the cathode structure by the TiO_2 coating (as evidenced by the suppressed Ni redox activity) paired with the extended 4.4 V plateau indicates an exacerbated structural rearrangement, whereas the ZnO and Cr_2O_3 coatings suppressed this behavior, perhaps by limiting the reaction of (104) planes with EC.[21] The Cr_2O_3-coated samples suppressed this reaction more than the ZnO and TiO_2 coatings, which correlated with longer cycle life and better capacity retention, indicating the importance of coating selection for high-voltage cycling. The ZnO-coated sample reached a slightly higher specific capacity of 170 mA h/g, but only the Cr_2O_3-coated sample achieved the theoretical specific capacity at 200 mA h/g. Each of the three cathode types had similar first cycle discharge capacities, with the Cr_2O_3-coated sample discharging 94 mA h/g and the TiO_2 and ZnO-coated samples providing 87 and 84 mA h/g, respectively. Based on the position of the primary plateau for the Cr_2O_3-coated sample being at the expected Ni redox center, the additional capacity was likely due to additional utilization of the bulk Li inventory rather than parasitic reactions. The uncoated 622 had the largest capacity due to the nonpassivating nature of the surface promoting electrochemical side reactions with the electrolyte.

All metal oxide-coated cell thin films studied here exhibited substantial capacity loss at a higher charge and discharge rate of 40 mA/g (∼C/5). These data are included in Figure 2b, where the Cr_2O_3-coated cells again exhibited the highest initial specific charge capacity at 32 mA h/g. The ZnO-coated sample had the highest coulombic efficiency at 95% in the 10th cycle, while the TiO_2-coated sample had the lowest at 81%. The voltage profiles had a similar shape between each sample (Figure S4). The massive loss in specific capacity (80+%) at

https://dx.doi.org/10.1021/acsomega.0c00458
ACS Omega 2020, 5, 14968−14975

higher charge and discharge rates was likely due to the irreversible structural change which is known to occur at the surface of NMC622 when cycled to high upper cutoff voltages and amplified in this thin-film configuration.[29] The 4.5 V *versus* Li/Li^+ cutoff voltage was chosen here to accentuate material degradation to study interfacial effects.

The inset of Figure 2c shows the impedance data for the pristine samples, with similar R_{el} (12−29 ohm·cm^2). Interfacial impedance (R_{ct} and R_{CEI}) was considered as one element for the pristine samples and may originate from charge-transfer resistance between the solvated Li^+ and metal oxide coatings at the electrode surface. After cycling, impedance components were more distinguishable than the sloping profile of the initial impedance, and so, they were fit according to the equivalent circuit model in the inset of Figure 2d corresponding to processes occurring in series in this cell. Resistance by the bulk electrolyte to Li^+ conduction in solution was represented by R_e, with desolvation of Li^+ at the interface and diffusion through the CEI in the high-frequency regime (R_{CEI} and Q_{CEI}), charge transfer impedance and double-layer capacitance at the NMC surface (R_{ct} and Q_{dl}), and a constant phase element for Li diffusion in the thin film (Q_b).[32]

ZnO-coated samples experienced the greatest impedance rise, from 85 ohm·cm^2 in the pristine sample to 490 ohm·cm^2 after cycling. Cr_2O_3 and TiO_2-coated cathodes had lower R_{CEI} values at 309 ohm·cm^2 and 207 ohm·cm^2, respectively. The same trend was observed in the impedance data after formation cycles. The evolution of R_{CEI} is plotted in Figure 2d; duplicates are shown in Figure S5. While Cr_2O_3 and ZnO-coated samples follow the trend of continuous impedance growth with cycling, R_{CEI} for the TiO_2-coated samples decreased between formation cycles and the end of cycling at C/5, which has been observed previously for NMC622 cycled to 4.4 V *versus* Li/Li^+ and may indicate a suppression of oxidative decomposition of the electrolyte.[5]

The electrodes were extracted from Swagelok cells after 2 cycles at 10 mA/g and 10 cycles at 40 mA/g and then transferred under vacuum to the XPS chamber for surface analysis. Thin-film electrodes enable a facilitated view of interfacial species in XPS because of the lack of binder and conductive carbon signals. The data for each of the metal oxide-coated samples are included in Figure 3 for both the pristine and cycled electrodes and were deconvoluted into component peaks based on pristine electrodes and Li salts, previously observed on our instrument. NMC622 films without metal oxide coatings are also included at the top in black as a reference. The C 1s spectra in Figure 3a highlight four primary peak components which were observed on all samples: aliphatic carbon and C−H bonds at 284.8 eV, C−O at 286.2 eV, O−C−O/C═O at 287.2 eV, and CO_3/O−C═O bonds at 288.9 eV. Each of the pristine metal oxide-coated electrodes had a greater at.% of CO_3-type bonds relative to the cycled samples, with the pristine TiO_2 sample (shown in red) having the most at 37 at. % of its C 1s signal. This larger proportion of CO_3 was reproducible in the all TiO_2 samples and may be due to carbonate formation from TiO_2 exposed to CO_2 which has been observed previously in the photocatalyst studies.[34]

Each electrode experienced an increase in the C−C/C−H and O−C−O peak contributions after cycling, suggesting the formation of polymerized species at the interface because of solvent decomposition. The ZnO-coated samples (shown in blue) had an additional minor C 1s contribution by the edge of the Zn(LMM) Auger line, which accounts for the asymmetric peak shape and broad component at ∼290.1 eV. The cycled uncoated NMC622 had an increase in the relative at. % of the CO_3 peak, which differed from all of the metal oxide-coated samples and suggests that the metal oxide coatings suppressed the formation or deposition of carbonate species.

The O 1s spectra in Figure 3b supported the observations of the C 1s spectra as well as suggested differences in the CEI thickness between samples. In each of the pristine samples, a peak at ∼529.8 eV originates from metal oxide bonds which were convoluted between the TiO_2, Cr_2O_3, and ZnO coatings and the NMC622 lattice contributions. This signal was reduced in intensity after cycling, indicating the formation of a CEI layer atop the M−O coatings. The Cr_2O_3-coated sample had the greatest M−O signal reduction at 87%, followed by the TiO_2-coated and ZnO-coated samples at 70%. This indicates that the CEI was thickest for the most acidic surface as it attenuated the M−O signal the most. The chemistry of the CEI was complex, with LiOR bonds observed at 530.8 eV, CO_3/O−C═O species at 531.5 eV, C−O bonds at 532.5 eV, and $Li_xPO_yF_z$ species at 533.7 eV.[35,36]

Only the cycled samples are included in the F 1s and P 2p spectra of Figure 3c,d because the pristine materials had no peaks above the background. The species observed in the F 1s spectra for each sample necessarily originate from the only fluorinated component of the system: $LiPF_6$, residual amounts of which can be observed at 688.3 eV despite the electrodes being gently rinsed in dimethyl carbonate (DMC) after extraction. The other contributions in the F 1s spectra of each sample were LiF at ∼685.1 eV and $Li_xPO_yF_z$ at ∼686.9 eV. Cr−F and Ti−F bonds may also contribute at ∼685 eV and will be discussed below. Because the absolute intensity detected in two different XPS samples can vary, it is important to consider the relative intensities of species within each sample. The ratio of these species varies between compounds, with a LiF/$Li_xPO_yF_z$ ratio of 1.97, 0.93, 1.09, and 2.72 for the uncoated, TiO_2, Cr_2O_3, and ZnO-coated cathodes, respectively. This difference in surface chemistry is supported by the P 2p spectra, where the relative amount of $Li_xPO_yF_z$ was similar in each case. This suggests that the amount of LiF detected at the surface was the primary difference in decomposed salt species at the surface. The more basic surface of the ZnO-coated electrode had almost three times more LiF/$Li_xPO_yF_z$ compared to the more acidic samples, suggesting that the more basic surface charge increases LiF formation. The more acidic surfaces may also suppress LiF formation by favoring CrF_3, TiF_4, or $TiOF_2$ formation, as their LiF/$Li_xPO_yF_z$ was about half that of the uncoated NMC and the Cr_2O_3 and TiO_2 samples had a shift in their respective spectra which will be discussed presently.

The metal oxide signals observed in the O 1s spectra can be further investigated in the Ti 2p, Cr 2p, and Zn 2p spectra of Figure 3e. In each case, the metal oxide signal was attenuated after cycling, indicating the formation of a CEI layer atop the coating. Interestingly, the degree of attenuation is different between samples, with the Cr 2p signal almost completely obstructed after cycling, followed by the Ti 2p signal, meaning that Cr species in the CEI are coated by other species. The Zn 2p signal retained a higher signal relative to the other metals. This suggests the thinnest CEI on ZnO followed by TiO_2 and Cr_2O_3 with the thickest layer. This trend of increasing CEI thickness aligns with the surface becoming more acidic. There was also a shift of the Cr $2p^{3/2}$ peak to a higher binding energy

https://dx.doi.org/10.1021/acsomega.0c00458
ACS Omega 2020, 5, 14968−14975

(from 576.3 to 578.7 eV), indicating either a transition from Cr^{3+} to Cr^{6+} or bonding with a more electronegative species (*i.e.,* F).[37] The Ti $2p^{3/2}$ peak had a more modest shift from 458.2 to 459.4, which may also indicate the formation of TiF_4 or $TiOF_2$.[38] This reaction of surface metal oxides with electrolyte salt species has previously been observed for Al_2O_3.[15] Interestingly, there was no shift of the Zn 2p peaks, indicating that the basic ZnO surface layer does not react to form fluorinated species or further oxidize as was the case for the more acidic surfaces of the TiO_2 and Cr_2O_3-coated samples.

A trend emerges when considering the XPS data alongside the impedance measurements: the cathode with a more basic surface created by the ZnO coating had higher impedance in all cases while having significantly more LiF and a thinner CEI relative to the more acidic samples. This suggests a more compact inorganic CEI induced by the basic surface, either because of increased salt decomposition or reduced solvent decomposition. Additionally, the metal oxide films of the more acidic surfaces reacted with the electrolyte to form fluorinated species or perhaps further oxidize, in the case of Cr_2O_3. This difference in the CEI composition correlates with the greater impedance increase and the poorer cycling performance of the more basic ZnO surface and aligns with the previous work finding that a thin, fluorinated CEI was preferable for high-voltage cycling of NMC622.[33] This trend of relative acidity validates theoretical calculations of C−H bond dissociation of EC on different organic surfaces by Shao-Horn *et al.*[39] This decomposition mechanism was shown to be more energetically favorable than the electrophilic or nucleophilic attack and indicated that metal fluorides which have a lower affinity for hydrogen would be preferable for minimizing EC decomposition. There has also been evidence in the recent literature that some coatings (*e.g.* Al_2O_3) outperforming other NMC622 coatings is due to a synergistic reaction of the coating with salt anions to form metal oxyfluorides.[3] $Li_2PO_2F_2$ may also form and has recently been identified as an effective electrolyte additive for capacity retention by forming a thin uniform CEI which passivates the cathode against continuous electrolyte decomposition at high voltages,[40,41] perhaps by forming Li_3PO_4 at the surface.[42] This supports the results described above because there was an increase in the $Li_xPO_yF_z$ signal for the metal oxide coatings which reacted with $LiPF_6$ to form metal fluoride or metal oxyfluoride in the CEI. A study of NMC622 pellets coated with Al_2O_3, TiO_2, or Nb_2O_5 also observed the formation of metal oxyfluoride species.[43] In that work, oxides which formed thicker layers of metal oxyfluorides had greater EC dehydrogenation and lower capacity retention than thinner layers of metal oxyfluorides.[43] This suggests that there may be an optimal CEI composition which is rich with metal fluorides or oxyfluorides while remaining sufficiently thin to minimize interfacial impedance. Furthermore, the differences in IEP of various Al_2O_3s might be a critical component to obtain the "most stable" surface of cathodes and should be considered by those investigating oxide coatings.

■ CONCLUSIONS

Metal oxide films of varying IEPs were deposited on NMC622 thin films to control the initial surface chemical environment and study its effects on CEI formation and evolution. The metal oxidation states determined by XPS confirmed the presence of ZnO, Cr_2O_3, and TiO_2 formed by dc sputtering of metal targets in an O_2/Ar environment. Zeta potential measurements of the coated cathodes found that the samples had increasing acidity in the order ZnO < TiO_2 < Cr_2O_3, which correlated to differences in the cycling performance and CEI composition. The most acidic sample (Cr_2O_3 coating) had the highest initial specific capacity and best capacity retention. The less-acidic TiO_2-coated sample had the lowest interfacial impedance after cycling, whereas the most basic sample (ZnO) had the highest impedance at all periods measured. The ZnO-coated sample also had a thinner CEI with a greater LiF concentration than the other samples, indicating that a more basic surface correlates with increased electrolyte salt decomposition but less solvent decomposition and higher impedance overall. The metal oxides of the more acidic samples were oxidized with cycling, possibly forming CrF_3 and TiF_4 or $TiOF_2$. The efficacy of Al_2O_3 coatings has also been attributed to the formation of AlF_3, suggesting that surface oxide layers which react with the electrolyte salt to form a highly fluorinated passivation layer are desirable. This suggests that the IEP of metal oxide coatings directly impacts electrolyte decomposition in high voltage operation of Ni-rich NMC, with more acidic surfaces preferred for better cycle life and increased cell capacity.

■ EXPERIMENTAL SECTION

Synthesis. Thin films of $LiNi_{0.6}Mn_{0.2}Co_{0.2}O_2$ (NMC622) were prepared by radio frequency magnetron sputtering of home-built NMC622 targets.[23] The deposition conditions in this study included a base chamber pressure <2 × 10^{-6} Torr with 55.0 sccm high-purity Ar gas (99.9995%, Airgas) flow rate, providing 6.0 mTorr deposition pressure at 90 W forward power. Following simultaneous deposition of 1 μm NMC622 onto 10 1 cm diameter Al_2O_3 substrates coated with Co and Pt, thin films were annealed at 700 °C for 1 h under high-purity air flow (∼0.2 LPM, Airgas) with a ramp rate of 5 °C/min then stored in an Ar-filled glove box. Metal oxide films (3 nm) were deposited on sintered NMC622 films by direct-current sputtering of Ti, Cr, or Zn metal (99.95−99.99% purity, Kurt J. Lesker) under 15 sccm Ar and 5 sccm O_2 at 20 mTorr and 30 W for durations according to their respective deposition rates, as measured by the quartz crystal micro-balance.

Characterization. Zeta potential of films was collected on a Brookhaven Zeta Potential Analyzer using Phase Analysis Light Scattering (ZetaPALS) with a Surface Zeta Potential probe attachment. The negative and positive probe particle solutions had pH values of 6.67 and 4.13, respectively. Reference standards were pellets of TiO_2 (Johnsen Matthey), Cr_2O_3 (Alfa Products, 98%), and ZnO (Alfa Aesar, Puratronic, 99.9995%) sintered at 1250 °C and direct current sputtered films (∼200 nm) of amorphous TiO_2, Cr_2O_3, and ZnO on 1 cm Al_2O_3 wafers. The IEP of each starting powder compound was measured by dispersing metal oxide powders in 1 mM KNO_3 and titrating with HNO_3 and NH_4OH for an array of solutions with a pH range of ∼2−10. The reported zeta potential data of each solution are an average of 100 measurements at 25.0 °C.

XPS was conducted on a PHI 3056 XPS spectrometer operated at 350 W and 15 kV with an Mg Kα (1253.6 eV) source. Pristine samples were transferred in air, and cycled films were transferred under vacuum for measurement in a cryo-pumped vacuum chamber at 10^{-9} Torr or less (10^{-11} Torr base pressure). Survey scans were collected at 93.9 eV pass energy with 0.5 eV energy steps, while high-resolution

https://dx.doi.org/10.1021/acsomega.0c00458
ACS Omega 2020, 5, 14968−14975

scans were acquired at 23.5 eV pass energy and 0.05 eV energy steps with 20−60 repeated scans of all spectra to improve the signal-to-noise ratio. Spectra were shifted relative to the adventitious carbon peak (284.8 eV) to correct for charging. Raw data were fit to the component peaks based on Li salts collected in the same instrument to provide standard references for the relative peak area, position, and full width at half maximum.

Electrochemical Measurements. Electrochemical cells were assembled in an Ar-filled glovebox in Swagelok cells *versus* Li metal (1 cm diameter). Two 1.3 cm diameter separators (Dreamweaver Gold 40) were soaked in 300 μL of 1.2 M $LiPF_6$ in EC and ethyl methyl carbonate in a 3:7 wt ratio (Tomiyama). The cells rested at an open-circuit voltage for 2 h before cycling for two formation cycles between 3.0 and 4.5 V *versus* Li/Li^+ in a constant current, constant voltage protocol (CC/CV). Constant current steps of 10 mA/g (∼C/20, where theoretical capacity is 200 mA h/g) were held until the upper cutoff voltage (UCV) followed by a constant potential hold at UCV until measured current dropped below 5 mA/g (C/40), and then, cells were discharged at 10 mA/g constant current to the lower cutoff voltage. This was followed by 10 CC/CV cycles at 40 mA/g (∼C/5) with the same cutoff limitations. Electrochemical impedance spectroscopy tests were conducted before and after the 2 formation cycles and after the 10 C/5 cycles on a BioLogic MPG-2 Battery Tester when cells were at an open-circuit voltage over 10 mHz to 20 kHz with an applied signal of 6 mV. The cycled electrodes were extracted in an Ar-filled glove box and rinsed with 1 mL of DMC (Aldrich, 99.95%) for 30 s before drying under vacuum and transferring to the XPS chamber under vacuum.

■ ASSOCIATED CONTENT

Supporting Information

The Supporting Information is available free of charge at https://pubs.acs.org/doi/10.1021/acsomega.0c00458.

Nickel 2p XPS, zeta potential, extended cycling, and Nyquist plots (PDF)

■ AUTHOR INFORMATION

Corresponding Authors

Nathan D. Phillip − *The Bredesen Center for Interdisciplinary Research and Graduate Education, University of Tennessee, Knoxville, Tennessee 37996, United States; Chemical Sciences Division, Oak Ridge National Laboratory, Oak Ridge, Tennessee 37831, United States;* orcid.org/0000-0002-6223-8765; Email: nathandphillip@gmail.com

Gabriel M. Veith − *Chemical Sciences Division, Oak Ridge National Laboratory, Oak Ridge, Tennessee 37831, United States;* orcid.org/0000-0002-5186-4461; Email: veithgm@ornl.gov

Authors

Beth L. Armstrong − *Materials Science and Technology Division, Oak Ridge National Laboratory, Oak Ridge, Tennessee 37831, United States;* orcid.org/0000-0001-7149-3576

Claus Daniel − *The Bredesen Center for Interdisciplinary Research and Graduate Education, University of Tennessee, Knoxville, Tennessee 37996, United States; Energy and Environmental Sciences Directorate, Oak Ridge National Laboratory, Oak Ridge, Tennessee 37831, United States*

Complete contact information is available at: https://pubs.acs.org/10.1021/acsomega.0c00458

Notes

The authors declare no competing financial interest.

■ ACKNOWLEDGMENTS

This research at the Oak Ridge National Laboratory, managed by UT Battelle, LLC, for the U.S. Department of Energy (DOE) under contract DE-AC05-00OR22725, was sponsored by the Office of Energy Efficiency and Renewable Energy (EERE) Vehicle Technologies Office (VTO) (Deputy Director: David Howell) Applied Battery Research subprogram (Program Manager: Peter Faguy) (N.D.P., C.D., and G.M.V.). A portion (IEP) was sponsored by the Office of Energy Efficiency and Renewable Energy (EERE) Vehicle Technologies Office (VTO) (Deputy Director: David Howell) Silicon Deep Dive subprogram (Program Manager: Brian Cunningham) (B.L.A.). The authors thank Alex Rogers and Katie Burdette for assistance with zeta potential data interpretation.

■ REFERENCES

(1) Han, B.; Key, B.; Lapidus, S. H.; Garcia, J. C.; Iddir, H.; Vaughey, J. T.; Dogan, F. From coating to dopant: how the transition metal composition affects alumina coatings on Ni-rich cathodes. *ACS Appl. Mater. Interfaces* **2017**, *9*, 41291−41302.

(2) Liu, W.; Li, X.; Xiong, D.; Hao, Y.; Li, J.; Kou, H.; Yan, B.; Li, D.; Lu, S.; Koo, A.; Adair, K.; Sun, X. Significantly improving cycling performance of cathodes in lithium ion batteries: the effect of Al_2O_3 and $LiAlO_2$ coatings on $LiNi_{0.6}Co_{0.2}Mn_{0.2}O_2$. *Nano Energy* **2018**, *44*, 111−120.

(3) Hall, D. S.; Gauthier, R.; Eldesoky, A.; Murray, V. S.; Dahn, J. R. New chemical insights into the beneficial role of Al_2O_3 cathode coatings in lithium-ion cells. *ACS Appl. Mater. Interfaces* **2019**, *11*, 14095−14100.

(4) Chen, Y.; Zhang, Y.; Chen, B.; Wang, Z.; Lu, C. An approach to application for $LiNi_{0.6}Co_{0.2}Mn_{0.2}O_2$ cathode material at high cutoff voltage by TiO_2 coating. *J. Power Sources* **2014**, *256*, 20−27.

(5) Gao, H.; Zeng, X.; Hu, Y.; Tileli, V.; Li, L.; Ren, Y.; Meng, X.; Maglia, F.; Lamp, P.; Kim, S.-J.; Amine, K.; Chen, Z. Modifying the surface of a high-voltage lithium-ion cathode. *ACS Appl. Energy Mater.* **2018**, *1*, 2254−2260.

(6) Gao, H.; Cai, J.; Xu, G.-L.; Li, L.; Ren, Y.; Meng, X.; Amine, K.; Chen, Z. Surface modification for suppressing interfacial parasitic reactions of nickel-rich lithium-ion cathode. *Chem. Mater.* **2019**, *31*, 2723−2730.

(7) Cheng, C.; Yi, H.; Chen, F. Effect of Cr_2O_3 coating on $LiNi_{1/3}Co_{1/3}Mn_{1/3}O_2$ as cathode for lithium-ion batteries. *J. Electron. Mater.* **2014**, *43*, 3681−3687.

(8) Şahan, H.; Göktepe, H.; Patat, Ş.; Ülgen, A. Effect of the Cr_2O_3 coating on electrochemical properties of spinel $LiMn_2O_4$ as a cathode material for lithium battery applications. *Solid State Ionics* **2010**, *181*, 1437−1444.

(9) Chang, W.; Choi, J.-W.; Im, J.-C.; Lee, J. K. Effects of ZnO coating on electrochemical performance and thermal stability of $LiCoO_2$ as cathode material for lithium-ion batteries. *J. Power Sources* **2010**, *195*, 320−326.

(10) Lai, Y.-Q.; Xu, M.; Zhang, Z.-A.; Gao, C.-H.; Wang, P.; Yu, Z.-Y. Optimized structure stability and electrochemical performance of $LiNi_{0.8}Co_{0.15}Al_{0.05}O_2$ by sputtering nanoscale ZnO film. *J. Power Sources* **2016**, *309*, 20−26.

(11) Baggetto, L.; Dudney, N. J.; Veith, G. M. Surface chemistry of metal oxide coated lithium manganese nickel oxide thin film cathodes studied by XPS. *Electrochim. Acta* **2013**, *90*, 135−147.

(12) Myung, S.-T.; Amine, K.; Sun, Y.-K. Surface modification of cathode materials from nano-to microscale for rechargeable lithium-ion batteries. *J. Mater. Chem.* **2010**, *20*, 7074−7095.
(13) Mohanty, D.; Dahlberg, K.; King, D. M.; David, L. A.; Sefat, A. S.; Wood, D. L.; Daniel, C.; Dhar, S.; Mahajan, V.; Lee, M.; Albano, F. Modification of Ni-rich FCG NMC and NCA cathodes by atomic layer deposition: preventing surface phase transitions for high-voltage lithium-ion batteries. *Sci. Rep.* **2016**, *6*, 26532.
(14) Li, X.; Liu, J.; Meng, X.; Tang, Y.; Banis, M. N.; Yang, J.; Hu, Y.; Li, R.; Cai, M.; Sun, X. Significant impact on cathode performance of lithium-ion batteries by precisely controlled metal oxide nano-coatings via atomic layer deposition. *J. Power Sources* **2014**, *247*, 57−69.
(15) Myung, S.-T.; Izumi, K.; Komaba, S.; Sun, Y.-K.; Yashiro, H.; Kumagai, N. Role of alumina coating on Li− Ni− Co− Mn− O particles as positive electrode material for lithium-ion batteries. *Chem. Mater.* **2005**, *17*, 3695−3704.
(16) Tian, C.; Lin, F.; Doeff, M. M. Electrochemical characteristics of layered transition metal oxide cathode materials for lithium ion batteries: surface, bulk behavior, and thermal properties. *Acc. Chem. Res.* **2018**, *51*, 89−96.
(17) Baggetto, L.; Unocic, R. R.; Dudney, N. J.; Veith, G. M. Fabrication and characterization of Li−Mn−Ni−O sputtered thin film high voltage cathodes for Li-ion batteries. *J. Power Sources* **2012**, *211*, 108−118.
(18) Moses, A. W.; Flores, H. G. G.; Kim, J.-G.; Langell, M. A. Surface properties of $LiCoO_2$, $LiNiO_2$ and $LiNi_{1-x}Co_xO_2$. *Appl. Surf. Sci.* **2007**, *253*, 4782−4791.
(19) Parks, G. A.; Bruyn, P. L. d. The zero point of charge of oxides. *J. Phys. Chem.* **1962**, *66*, 967−973.
(20) Parks, G. A. The isoelectric points of solid oxides, solid hydroxides, and aqueous hydroxo complex systems. *Chem. Rev.* **1965**, *65*, 177−198.
(21) Xu, S.; Luo, G.; Jacobs, R.; Fang, S.; Mahanthappa, M. K.; Hamers, R. J.; Morgan, D. Ab initio modeling of electrolyte molecule ethylene carbonate decomposition reaction on $Li(Ni,Mn,Co)O_2$ cathode surface. *ACS Appl. Mater. Interfaces* **2017**, *9*, 20545−20553.
(22) Paulsen, J.; Kim, J. High Nickel Cathode Material Having Low Soluble Base Content. U.S. Patent 9,698,418B2, 2017.
(23) Phillip, N. D.; Ruther, R. E.; Sang, X.; Wang, Y.; Unocic, R. R.; Westover, A. S.; Daniel, C.; Veith, G. M. Synthesis of Ni-Rich Thin-Film Cathode as Model System for Lithium Ion Batteries. *ACS Appl. Energy Mater.* **2019**, *2*, 1405−1412.
(24) Veith, G. M.; Lupini, A. R.; Baggetto, L.; Browning, J. F.; Keum, J. K.; Villa, A.; Prati, L.; Papandrew, A. B.; Goenaga, G. A.; Mullins, D. R.; Bullock, S. E.; Dudney, N. J. Evidence for the Formation of Nitrogen-Rich Platinum and Palladium Nitride Nanoparticles. *Chem. Mater.* **2013**, *25*, 4936−4945.
(25) Moulder, J. F.; Stickle, W. F.; Sobol, P. E.; Bomben, K. D. *Handbook of X-ray Photoelectron Spectroscopy*; Perkin-Elmer Corporation: Eden Prairie, Minnesota, 1995; pp 230−232.
(26) Grohmann, I.; Kemnitz, E.; Lippitz, A.; Unger, W. E. S. Curve fitting of Cr 2p photoelectron spectra of Cr_2O_3 and CrF_3. *Surf. Interface Anal.* **1995**, *23*, 887−891.
(27) Kittaka, S. Isoelectric point of Al_2O_3, Cr_2O_3 and Fe_2O_3. I. Effect of heat treatment. *J. Colloid Interface Sci.* **1974**, *48*, 327−333.
(28) Bhattacharjee, S. DLS and zeta potential−what they are and what they are not? *J. Controlled Release* **2016**, *235*, 337−351.
(29) Tian, C.; Nordlund, D.; Xin, H. L.; Xu, Y.; Liu, Y.; Sokaras, D.; Lin, F.; Doeff, M. M. Depth-dependent redox behavior of $LiNi_{0.6}Mn_{0.2}Co_{0.2}O_2$. *J. Electrochem. Soc.* **2018**, *165*, A696−A704.
(30) Jung, R.; Metzger, M.; Maglia, F.; Stinner, C.; Gasteiger, H. A. Oxygen release and its effect on the cycling stability of $LiNi_xMn_yCo_zO_2$ (NMC) cathode materials for Li-ion batteries. *J. Electrochem. Soc.* **2017**, *164*, A1361−A1377.
(31) Phillip, N. D.; Westover, A. S.; Daniel, C.; Veith, G. M. Structural Degradation of High Voltage Lithium Nickel Manganese Cobalt Oxide (NMC) Cathodes in Solid-State Batteries and Implications for Next Generation Energy Storage. *ACS Appl. Energy Mater.* **2020**, *3*, 1768−1774.
(32) Levi, M. D.; Salitra, G.; Markovsky, B.; Teller, H.; Aurbach, D.; Heider, U.; Heider, L. Solid-state electrochemical kinetics of Li-Ion intercalation into $Li_{1-x}CoO_2$: simultaneous application of electro-analytical techniques SSCV, PITT, and EIS. *J. Electrochem. Soc.* **1999**, *146*, 1279−1289.
(33) Phillip, N. D.; Westover, A. S.; Daniel, C.; Veith, G. M. Structural Degradation of High Voltage Lithium Nickel Manganese Cobalt Oxide (NMC) Cathodes in Solid-State Batteries and Implications for Next Generation Energy Storage. *ACS Appl. Energy Mater.* **2020**, *3*, 1768−1774.
(34) Clark, J. C.; Dai, S.; Overbury, S. H. Operando studies of desorption, reaction and carbonate formation during CO oxidation by Au/TiO_2 catalysts. *Catal. Today* **2007**, *126*, 135−142.
(35) Hou, P.; Li, F.; Sun, Y.; Li, H.; Xu, X.; Zhai, T. Multishell precursors facilitated synthesis of concentration-gradient nickel-rich cathodes for long-life and high-rate lithium-ion batteries. *ACS Appl. Mater. Interfaces* **2018**, *10*, 24508−24515.
(36) Hou, P.; Yin, J.; Ding, M.; Huang, J.; Xu, X. Surface/interfacial structure and chemistry of high-energy nickel-rich layered oxide cathodes: advances and perspectives. *Small* **2017**, *13*, 1701802.
(37) Shuttleworth, D. Preparation of metal-polymer dispersions by plasma techniques. An ESCA investigation. *J. Phys. Chem.* **1980**, *84*, 1629−1634.
(38) Jain, A.; Agarwal, S.; Kumar, S.; Yamaguchi, S.; Miyaoka, H.; Kojima, Y.; Ichikawa, T. How does TiF_4 affect the decomposition of MgH_2 and its complex variants?−An XPS investigation. *J. Mater. Chem. A* **2017**, *5*, 15543−15551.
(39) Giordano, L.; Østergaard, T. M.; Muy, S.; Yu, Y.; Charles, N.; Kim, S.; Zhang, Y.; Maglia, F.; Jung, R.; Lund, I.; Rossmeisl, J.; Shao-Horn, Y. Ligand-dependent energetics for dehydrogenation: Implications in Li-ion battery electrolyte stability and selective oxidation catalysis of hydrogen-containing molecules. *Chem. Mater.* **2019**, *31*, 5464−5474.
(40) Wang, C.; Yu, L.; Fan, W.; Liu, J.; Ouyang, L.; Yang, L.; Zhu, M. Lithium difluorophosphate as a promising electrolyte lithium additive for high-voltage lithium-ion batteries. *ACS Appl. Energy Mater.* **2018**, *1*, 2647−2656.
(41) Hong, S.; Hong, B.; Song, W.; Qin, Z.; Duan, B.; Lai, Y.; Jiang, F. Communication-Lithium Difluorophosphate as an Electrolyte Additive to Improve the High Voltage Performance of LiNi0.5-Co0.2Mn0.3O2/Graphite Cell. *J. Electrochem. Soc.* **2018**, *165*, A368−A370.
(42) Zhao, W.; Zheng, G.; Lin, M.; Zhao, W.; Li, D.; Guan, X.; Ji, Y.; Ortiz, G. F.; Yang, Y. Toward a stable solid-electrolyte-interfaces on nickel-rich cathodes: $LiPO_2F_2$ salt-type additive and its working mechanism for $LiNi_{0.5}Mn_{0.25}Co_{0.25}O_2$ cathodes. *J. Power Sources* **2018**, *380*, 149−157.
(43) Karayaylali, P.; Tatara, R.; Zhang, Y.; Chan, K.-L.; Yu, Y.; Giordano, L.; Maglia, F.; Jung, R.; Lund, I.; Shao-Horn, Y. Editors' Choice-Coating-Dependent Electrode-Electrolyte Interface for Ni-Rich Positive Electrodes in Li-Ion Batteries. *J. Electrochem. Soc.* **2019**, *166*, A1022−A1030.

https://dx.doi.org/10.1021/acsomega.0c00458
ACS Omega 2020, 5, 14968−14975